Deficiency in the secreted protein Semaphorin3d causes abnormal parathyroid development in mice

Received for publication, December 7, 2018, and in revised form, April 9, 2019 Published, Papers in Press, April 12, 2019, DOI 10.1074/jbc.RA118.007063

Anamika Singh[‡1], **Masum M. Mia**[‡1], **Dasan Mary Cibi**[‡], **Ashutosh Kumar Arya**[§], **Sanjay Kumar Bhadada**[§], and **Manvendra K. Singh**[‡¶2]

From the [‡]*Program in Cardiovascular and Metabolic Disorders, Duke-NUS Medical School Singapore, Singapore 169857, the* [¶]*National Heart Research Institute Singapore, National Heart Center Singapore, Singapore 169609, and the* [§]*Department of Endocrinology, Postgraduate Institute of Medical Education and Research (PGIMER), Chandigarh 160012, India*

Edited by Eric R. Fearon

Primary hyperparathyroidism (PHPT) is a common endocrinopathy characterized by hypercalcemia and elevated levels of parathyroid hormone. The primary cause of PHPT is a benign overgrowth of parathyroid tissue causing excessive secretion of parathyroid hormone. However, the molecular etiology of PHPT is incompletely defined. Here, we demonstrate that semaphorin3d (Sema3d), a secreted glycoprotein, is expressed in the developing parathyroid gland in mice. We also observed that genetic deletion of *Sema3d* leads to parathyroid hyperplasia, causing PHPT. *In vivo* and *in vitro* experiments using histology, immunohistochemistry, biochemical, RT-qPCR, and immunoblotting assays revealed that Sema3d inhibits parathyroid cell proliferation by decreasing the epidermal growth factor receptor (EGFR)/Erb-B2 receptor tyrosine kinase (ERBB) signaling pathway. We further demonstrate that EGFR signaling is elevated in *Sema3d*$^{-/-}$ parathyroid glands and that pharmacological inhibition of EGFR signaling can partially rescue the parathyroid hyperplasia phenotype. We propose that because Sema3d is a secreted protein, it may be possible to use recombinant Sema3d or derived peptides to inhibit parathyroid cell proliferation causing hyperplasia and hyperparathyroidism. Collectively, these findings identify Sema3d as a negative regulator of parathyroid growth.

The parathyroid glands synthesize and secrete parathyroid hormone (PTH)[3] to regulate serum calcium concentration in the body (1–4). In mice, there are two parathyroid glands located bilaterally in the neck and near the superior border of the thyroid gland. The parathyroid glands develop from the common parathyroid/thymus primordia, derived from the third pharyngeal pouch (5, 6). As the development proceeds, parathyroid is separated from the thymus and becomes situated near or embedded within the thyroid gland (7, 8). The early development and patterning of the parathyroid and thymus domains are controlled by a set of common regulatory genes (9–13). However, once the domains are specified within the same primordium, parathyroid cells express specific transcription factors such as glial cells missing 2 (Gcm2) (8). *Gcm2* is essential for the differentiation and survival of parathyroid cells. Mice with *Gcm2* deficiency develop aparathyroid phenotype because their parathyroid precursor cells fail to proliferate and differentiate and die via programmed cell death (8, 14, 15). Parathyroid hormone (*PTH*) gene expression is detected in the parathyroid domain before its separation from the thymus and is maintained throughout development (14).

Primary hyperparathyroidism (PHPT) is a common endocrine disorder caused by excessive secretion of PTH from the parathyroid glands (16, 17). PHPT is the third most common endocrine disorder, with a prevalence of 0.1–1.0%. It is more common in elderly females, with a prevalence of up to 2.1% in postmenopausal women (16, 18). In most cases of nonfamilial origin PHPT, hyperparathyroidism results from either benign single adenoma (80–85% cases) or multiglandular parathyroid hyperplasia (15–20% cases) (16, 17). In rare cases (<1%), parathyroid carcinoma has been associated with PHPT (19). The parathyroid gland maintains calcium homeostasis by sensing fluctuations in extracellular calcium levels through the calcium-sensing receptor (CaSR) and responding to changes in PTH secretion (1–4). PHPT is characterized by increased parathyroid cell proliferation and calcium-insensitive hypersecretion of parathyroid hormone (20). Another form of hyperparathyroidism is secondary hyperparathyroidism (SHPT), in which parathyroid glands become enlarged and hyperactive in response to a condition outside of the parathyroid causing hypocalcemia. SHPT is most frequently seen in patients with chronic kidney disease (21). In most primary or secondary hyperparathyroidism cases, increased serum PTH levels are associated with increased serum calcium levels, causing complications such as renal stones, neuropsychiatric disorders, and bone abnormalities (16). Parathyroidectomy is the most common treatment for hyperparathyroidism. However, reoperative

This work was supported by funds from Duke-NUS Medical School Singapore, the Goh Foundation, and Singapore National Research Foundation (NRF) Fellowship NRF-NRFF2016-01 (to M. K. S.). The authors declare that they have no conflicts of interest with the contents of this article.

This article contains Figs. S1–S3.

[1] Both authors contributed equally to this work.

[2] To whom correspondence should be addressed: Program in Cardiovascular and Metabolic Disorders, Duke-NUS Medical School Singapore, Singapore 169857. Tel.: 65-6601-3098; Fax: 65-6221-2534; E-mail: manvendra.singh@duke-nus.edu.sg.

[3] The abbreviations used are: PTH, parathyroid hormone; PHPT, primary hyperparathyroidism; CaSR, calcium-sensing receptor; SHPT, secondary hyperparathyroidism; E, embryonic day; P, postnatal day; qPCR, quantitative PCR; X-gal, 5-bromo-4-chloro-3-indolyl β-D-galactoside; CDK, cyclin-dependent kinase; CDKI, CDK inhibitor; EGF, epidermal growth factor; EGFR, EGF receptor; DMEM, Dulbecco's modified Eagle's medium; FBS, fetal bovine serum; DAPI, 4′,6-diamidino-2-phenylindole; AP, alkaline phosphatase; ANOVA, analysis of variance; RTK, receptor tyrosine kinase.

treatment for persistent or recurrent hyperparathyroidism remains technically challenging due to fibrotic scar and distorted anatomy that make it more difficult to identify the abnormal parathyroid glands (17, 22).

Semaphorins are highly conserved secreted membrane-bound glycoproteins originally identified as axon guidance molecules in the developing nervous system (23). However, work in recent years has implicated them in a wide range of developmental, physiological, and pathological processes outside of the central nervous system, including tumor progression (24–26). The primary receptors for semaphorins are plexins and neuropilins. Most membrane-bound semaphorins bind directly to plexins, whereas secreted class 3 semaphorins may require neuropilin as obligate plexin co-receptors (26, 27). Increasing evidence has shown that semaphorins also can signal through a nonplexin receptor complex (28, 29).

We have previously shown that Sema3d is expressed in the proepicardial organs and Sema3d-expressing proepicardial cells give rise to coronary vascular endothelium. While studying epicardial function of *Sema3d*, we noticed that Sema3d was expressed in the third pharyngeal pouch, giving rise to the parathyroid gland. Here, we report that Sema3d is expressed in the developing parathyroid gland and required for its proper development. Genetic deletion of *Sema3d* leads to PHPT due to the enlarged parathyroid gland. Molecular and biochemical analyses suggest that Sema3d inhibits parathyroid cell proliferation by decreasing the EGFR/ErbB signaling pathway. We demonstrate that EGFR signaling is elevated in $Sema3d^{-/-}$ parathyroid glands, and pharmacological inhibition of EGFR signaling can partially rescue the parathyroid hyperplasia phenotype. Because EGFR/ErbB signaling pathway is activated in the parathyroid glands in both PHPT and SHPT, the Sema3d-EGFR/ErbB signaling axis may be targeted to treat parathyroid hyperplasia, especially in persistent or recurrent hyperparathyroidism after parathyroidectomy.

Results

Sema3d-deficient mice develop primary hyperparathyroidism

To determine the expression of Sema3d during parathyroid development, we performed expression and lineage tracing analyses in $Sema3d^{GFPCre/+}$ mice (30). Bright field and direct GFP fluorescence in E9.5 $Sema3d^{GFPCre/+}$ embryos demonstrated that Sema3d is expressed in the third pharyngeal pouch. Stronger GFP signals were observed in the dorso-anterior domain of the third pouch that represents the parathyroid domain (Fig. 1*A*). Similarly, when we crossed the $Sema3d^{GFPCre/+}$ line with the $R26R^{lacZ}$ reporter line, strong β-gal activity was observed in the third pharyngeal pouch (Fig. 1*B*). Our results are consistent with a previous report suggesting that Sema3d is expressed in the parathyroid-specific domain of the common primordium that gives rise to the thymus and parathyroid (31). Thus far, $Sema3d^{-/-}$ mice survive and have abnormal pulmonary vein patterning causing left-to-right shunt, as characterized by severely enlarged right atria and ventricle (30). To demonstrate the functional requirement of Sema3d in parathyroid development, we performed histological and molecular analyses on the parathyroid gland in both

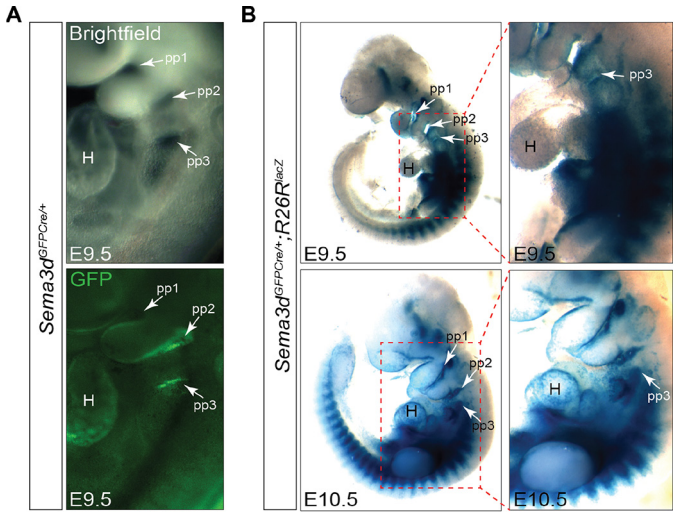

Figure 1. Sema3d expression in the developing third pharyngeal pouch. *A*, bright field and direct GFP fluorescence in E9.5 $Sema3d^{GFPCre/+}$ mouse embryos. *B*, whole-mount X-gal staining of E9.5 and E10.5 $Sema3d^{GFPCre/+}$; $R26R^{LacZ}$ embryos. *pp1*, pharyngeal pouch 1; *pp2*, pharyngeal pouch 2; *pp3*, pharyngeal pouch 3; *H*, heart.

control and $Sema3d^{-/-}$ mice. Morphological and histological examinations of the parathyroid glands from postnatal day 0 (P0), P6, and 12-month-old control and $Sema3d^{-/-}$ mice revealed a marked increase in size and hypercellularity, suggesting hyperplasia (Fig. 2, *A* and *B* and Fig. S1). Only one of the two parathyroid glands was hyperplastic, suggesting adenomatous transformation. Gross morphological and histological abnormalities resembling parathyroid hyperplasia were observed in 40% (19 of 46) of $Sema3d^{-/-}$ mice. Gcm2 immunohistochemistry was performed to mark the parathyroid glands in control and $Sema3d^{-/-}$ mice (Fig. 2*C*). Significant increase in the parathyroid area was observed in $Sema3d^{-/-}$ mice (Fig. 2*D*).

To determine whether parathyroid hyperplasia in $Sema3d^{-/-}$ mice leads to hyperparathyroidism, we measured serum PTH in 6-month-old mice. We observed elevated PTH levels in $Sema3d^{-/-}$ mice compared with their littermate controls (Fig. 2*E*). In most cases of PHPT, increased serum PTH levels are associated with increased serum calcium levels. However, in some cases of normocalcemic PHPT, PTH levels are elevated but serum calcium levels remain normal (18, 32). To determine whether elevated PTH levels in $Sema3d^{-/-}$ mice are associated with changes in calcium levels, we measured serum calcium levels in the same set of animals. We observed elevated calcium levels in $Sema3d^{-/-}$ mice compared with their littermate controls, suggesting PHPT (Fig. 2*F*). To determine the molecular changes associated with parathyroid hyperplasia, we isolated RNA from dissected parathyroid gland from control and $Sema3d^{-/-}$ mice and performed qPCR analysis for parathyroid-specific genes such as parathyroid hormone (*PTH*), glial cells missing homolog 2 (*Gcm2*), and calcium-sensing receptor (*CaSR*). Expression levels of *PTH* and *Gcm2* were significantly elevated in $Sema3d^{-/-}$ parathyroid compared with controls. However, the expression of *CaSR* was not altered in $Sema3d^{-/-}$ parathyroid glands (Fig. 2*G*).

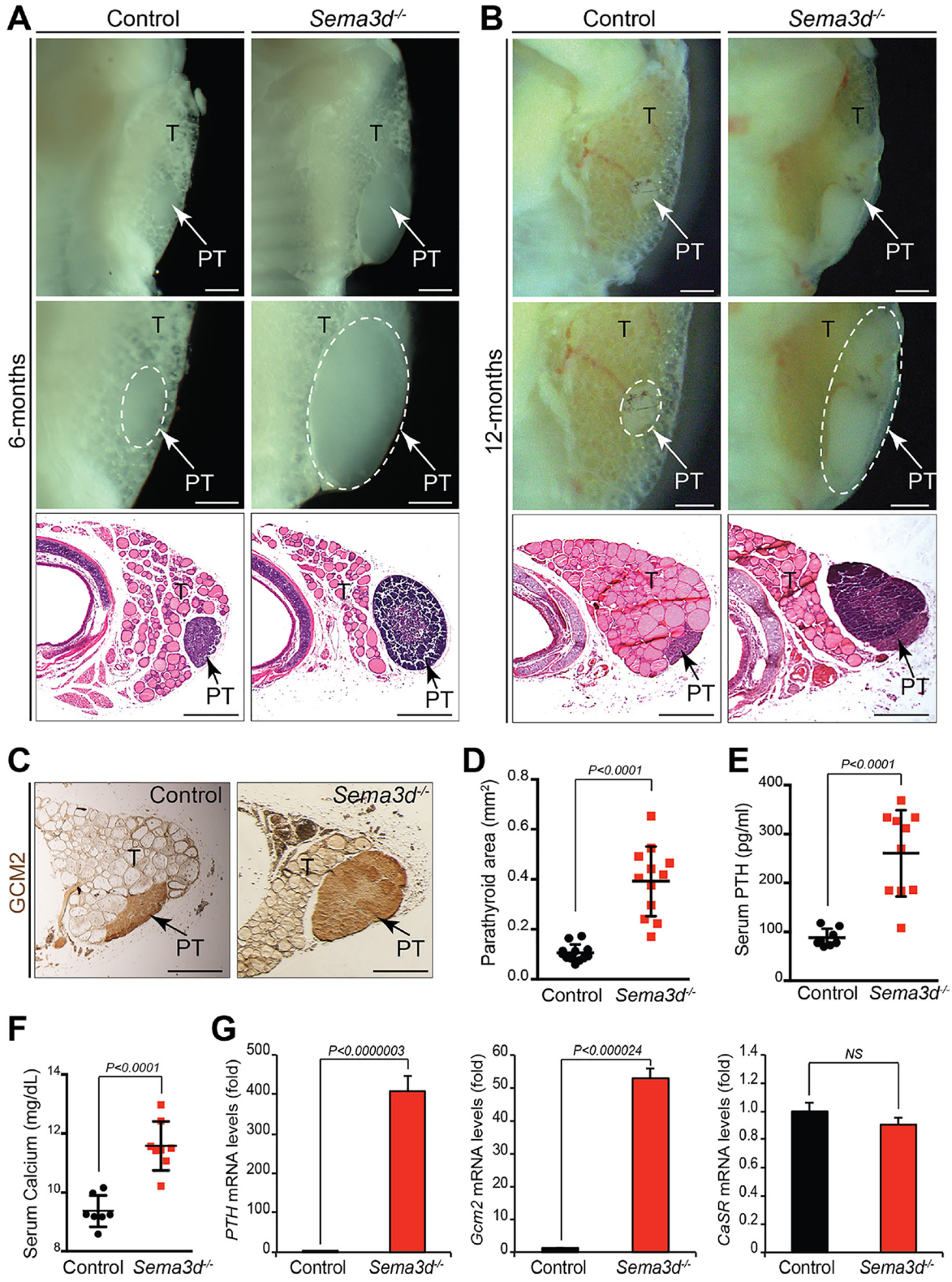

Figure 2. Primary hyperparathyroidism in *Sema3d*$^{-/-}$ mice. *A* and *B*, morphological and histological examination of parathyroid glands from 6- ($n = 12$ per genotype) and 12-month-old ($n = 15$ per genotype) control and *Sema3d*$^{-/-}$ mice. *C*, GCM2 immunohistochemistry on parathyroid sections from 12-month-old control and *Sema3d*$^{-/-}$ mice. *D*, quantification of parathyroid area in 12-month-old control and *Sema3d*$^{-/-}$ mice ($n = 12$). *E*, serum PTH levels in 12-month-old control ($n = 8$) and *Sema3d*$^{-/-}$ mice ($n = 10$). *F*, serum calcium levels in 12-month-old control ($n = 7$) and *Sema3d*$^{-/-}$ mice ($n = 8$). *G*, real-time qPCR for *PTH*, *Gcm2*, and *CaSR* on RNA isolated from the microdissected parathyroid gland of 6-month-old control ($n = 3$) and *Sema3d*$^{-/-}$ mice ($n = 3$). -Fold changes in gene expression are presented. *T*, thyroid; *PT*, parathyroid. *Scale bars*, 200 μm. *Error bars*, S.D.

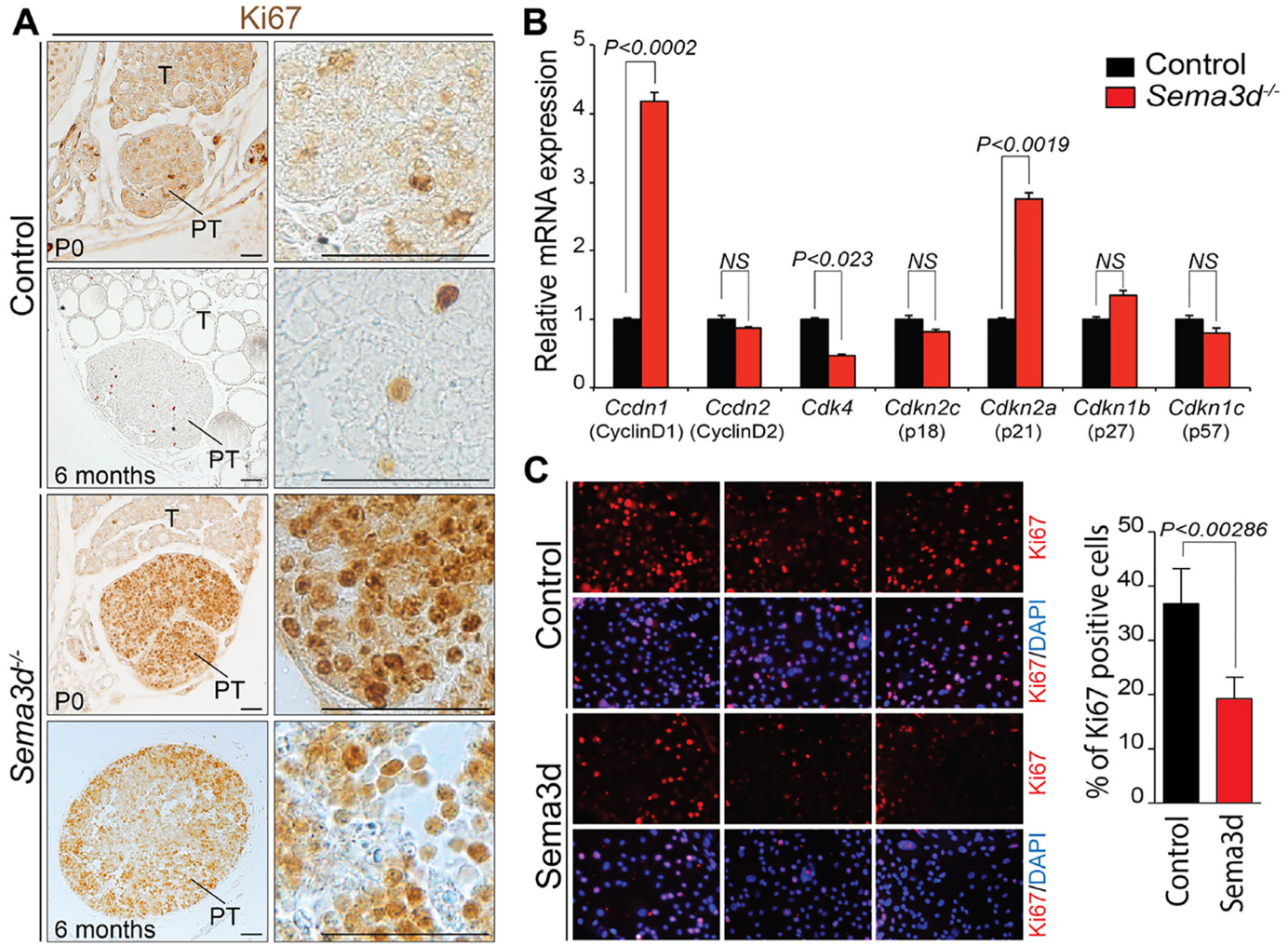

Figure 3. Sema3d inhibits parathyroid cell proliferation *in vivo* and *in vitro*. *A*, immunohistochemistry for Ki-67 on parathyroid sections from P0 and 6-month-old control ($n = 5$) and *Sema3d*$^{-/-}$ ($n = 5$) mice. High-magnification images show nuclear Ki-67 staining. *Scale bars*, 50 μm. *B*, real-time qPCR for cell cycle regulators, such as *Ccdn1*, *Ccdn1*, *Cdk4*, *Cdkn2c*, *Cdkn2a*, *Cdkn1b*, and *Cdkn1c* on RNA isolated from the microdissected parathyroid gland of 6-month-old control ($n = 3$) and *Sema3d*$^{-/-}$ mice ($n = 3$). *C*, immunostaining for Ki-67 on sHPT cells treated with control or recombinant Sema3d for 48 h. Nuclei were visualized by DAPI staining (*blue*), and the percentage of Ki-67–positive cells was quantified. *T*, thyroid; *PT*, parathyroid. *Error bars*, S.D.

Sema3d inhibits parathyroid cell proliferation

To determine whether observed hyperplasia in *Sema3d*$^{-/-}$ mice is due to abnormal parathyroid cell proliferation, we performed Ki-67 immunostaining on P0 and 6-month-old parathyroid sections from control and *Sema3d*$^{-/-}$ mice. A dramatic increase in the number of Ki-667–positive cells was noted in the *Sema3d*$^{-/-}$ parathyroid sections compared with controls at both time points. This suggests that abnormal cell proliferation is the primary cause of parathyroid hyperplasia (Fig. 3*A*). To determine the molecular changes associated with increased parathyroid cell proliferation and hyperplasia in *Sema3d*$^{-/-}$ mice, we analyzed the expression of cell cycle regulators, including cyclins, cyclin-dependent kinases (CDKs), and cyclin-dependent kinase inhibitor (CDKIs) by qPCR on RNA isolated from microdissected parathyroid glands. We observed a 4-fold increase in the expression of *Ccdn1* (cyclin D1), an oncogene known to be overexpressed in 20–40% of parathyroid adenomas (33–35). We also observed an increase in *Cdkn2a* (*p21*) and a modest decrease in *Cdk4* expression in *Sema3d*$^{-/-}$ parathyroid (Fig. 3*B*). Increased expression of *Cdkn2a* has been associated with tumor progression (36). Growing evidence suggests that, depending on its environment, *Cdkn2a* can act as either tumor suppressor or an oncogene (37, 38). No significant changes were observed in *Ccdn2* (cyclin D2), *Cdkn2c (p18)*, *Cdkn1b (p27)*, and *Cdkn1c (p57)*. To determine total RNA quality isolated from the microdissected parathyroid tissues, we performed qPCR analysis for thyroid-stimulating hormone receptor (*TSHR*), troponin T1 (*Tnnt1*), and *Sox9*. This allowed us to detect possible contamination from thyroid, skeletal muscle, and cartilage tissues, respectively. No significant changes were observed (Fig. S2). Together, these results suggest that Sema3d inhibits parathyroid cell proliferation *in vivo* by regulating the expression of cell cycle genes.

Because parathyroid tissues from mice are limited, we used a human parathyroid cell line, sHPT-1, to dissect the molecular mechanism of Sema3d-mediated inhibition of parathyroid cell proliferation. sHPT-1 is established from a hyperplastic parathyroid gland surgically removed from an SHPT patient (39). To determine whether sHPT-1 cells are sufficiently similar to primary parathyroid cells with regard to their semaphorin sig-

naling pathways, we treated sHPT-1 cells with recombinant Sema3d and analyzed proliferation by Ki-67 staining. Consistent with the *in vivo* data, we see significant reduction in sHPT-1 cell proliferation in Sema3d-treated samples compared with controls. This suggests that Sema3d inhibits parathyroid cell proliferation under both *in vivo* and *in vitro* conditions (Fig. 3*C*).

Sema3d inhibits EGFR signaling pathway to control parathyroid cell proliferation

Semaphorins signal through their classical Plexin and neuropilin receptors and other receptors, such as receptor tyrosine kinases (28, 40, 41). Sema3d binds and signals through Neuropilin-1 (Nrp1) to regulate endothelial cell patterning during pulmonary vein development (30, 42). However, Nrp1 is not expressed during parathyroid development, suggesting that Sema3d may signal through other receptors expressed by the parathyroid gland (31). In a candidate-based screening, we found that Sema3d inhibits the epidermal growth factor receptor (EGFR) signaling pathway. EGFR is a member of the ErbB family of receptor tyrosine kinases that includes ErbB2, ErbB3, and ErbB4. Ligand binding induces homo- or heterodimerization of EGFR with other family members, including ErbB2, and activation of intracellular tyrosine kinase through formation of an asymmetric kinase dimer. Activation of ErbB receptors results in activation of mitogen-activated protein kinase and phosphatidylinositol 3-kinase/Akt signaling, leading to enhanced proliferation, primarily due to aberrant changes in cell cycle gene expression, including cyclin D1 (43, 44). Enhanced EGFR signaling has been associated with parathyroid adenomas and hyperplasia in both PHPT and SHPT (45–49).

To determine whether Sema3d inhibits parathyroid cell proliferation through the EGFR signaling pathway, we treated sHPT-1 cells with control and alkaline phosphatase (AP)-tagged Sema3d (Sema3d-AP) conditioned medium and analyzed the expression of EGFR signaling components, such as pEGFR-Y1045, pEGFR-Y992, EGFR, pErbB2-Y1248, ErbB2, pAkt, Akt, pErk1/2, Erk1/2, and cyclin D1, by Western blotting. Sema3d-AP conditioned medium treatment reduced the amount of total EGFR, as well as pEGFR-Y1045 and pEGFR-Y992, suggesting that Sema3d may inhibit EGFR signaling by inducing receptor endocytosis/internalization and degradation. In parallel with EGFR down-regulation, ErbB2 and pErbB2-Y1248 levels were also decreased after nanomolar quantities of Sema3d treatment. To determine whether the downstream components of EGFR pathway were also affected after Sema3d treatment, we analyzed expression and activation of Akt and Erk1/2. The phosphorylation level of Akt and Erk1/2 was reduced. However, the total amount of Akt and Erk1/2 was not changed. Cyclin D1, one of the known targets of ErbB signaling in cancer cells, was significantly reduced in Sema3d-AP–treated cells (Fig. 4*A*). Next, we treated sHPT-1 cells with recombinant Sema3d at different time points and analyzed EGFR signaling components. Consistent with earlier observation, all signaling components were significantly down-regulated after Sema3d treatment (Fig. 4*B*). Treatment of sHPT-1 cells with increasing recombinant Sema3d concentrations affected the EGFR signaling pathway in a manner similar to that described above (Fig. 4, *C* and *D*).

Inhibitory effects of Sema3d on ErbB2 are EGFR-dependent

Although Sema3d does not bind to ErbB2 alone, it can bind as part of a receptor complex. This suggests that changes in pErbB2 levels in sHPT cells after Sema3d treatment were likely from the impact of EGFR signaling pathway (Fig. 4 and Fig. S3) (29). To determine whether the inhibitory effect of Sema3d on ErbB2 activation was EGFR-dependent, we co-transfected HEK293T cells with WT ErbB2 and a plasmid expressing either WT EGFR or kinase-inactive EGFR. The transfected cells were then treated with recombinant epidermal growth factor (EGF) in the presence/absence of Sema3d. Consistent with previous observations, when WT EGFR and WT ErbB2 were co-expressed, both receptors were phosphorylated in response to EGF (Fig. 4*E*). Sema3d exposures inhibited EGF-induced phosphorylation of both EGFR and ErbB2. However, when kinase-inactive EGFR and WT ErbB2 were co-expressed, no EGFR phosphorylation and a low level of ErbB2 phosphorylation were observed after EGF stimulation (Fig. 4*E*). The addition of Sema3d did not change ErbB2 phosphorylation, suggesting that the inhibitory effect of Sema3d on ErbB2 activation is EGFR-dependent (Fig. 4*E*).

Next, we tested whether Sema3d can inhibit the EGFR-activated pathway, a condition associated with parathyroid hyperplasia in both PHPT and SHPT (45–49). We treated sHPT-1 cells with different doses of NSC 228155, an EGFR activator (50), and performed Western blotting analyses on pEGFR-Y1045 and pEGFR-Y992 to determine the optimal dose required to activate the pathway. We observed that 100 μM NSC 228155 significantly increased the level of pEGFRs (Fig. 5*A*). Recombinant Sema3d inhibited NSC 228155–induced EGFR activation (Fig. 5*B*). Cyclin D1 expression was also increased with NSC 228155 treatment, but it was decreased following Sema3d treatment (Fig. 5*B*). To determine whether increased cyclin D1 expression correlated with increased cell proliferation, we treated sHPT-1 cells with NSC 228155 in the presence/absence of recombinant Sema3d and analyzed their proliferation (Fig. 5*C*). Activation of the EGFR pathway by NSC 228155 resulted in a significantly increased proportion (>80%, $p < 0.001$) of Ki-67–positive cells. However, the addition of Sema3d significantly decreased (~30%, $p < 0.001$) the number of Ki-67–positive cells induced by NSC 228155 treatment. This suggests that Sema3d regulates cell cycle progression by signaling through the EGFR (Fig. 5*C*). Together, both *in vivo* and *in vitro* results suggest that Sema3d inhibits the EGFR signaling pathway to restrict parathyroid cell proliferation. A recent study by Aghajanian *et al.* (29) demonstrated that Sema3d activates the ErbB2 signaling pathway in endothelial cells during coronary vasculature patterning. This indicates that, depending on its biological context, Sema3d can act as either agonists or antagonists for the ErbB signaling pathway (29).

Blocking EGFR signaling can partially rescue the parathyroid hyperplasia phenotype in Sema3d$^{-/-}$ mice

To determine whether Sema3d inhibits the EGFR pathway *in vivo*, pEGFR immunohistochemistry was performed on para-

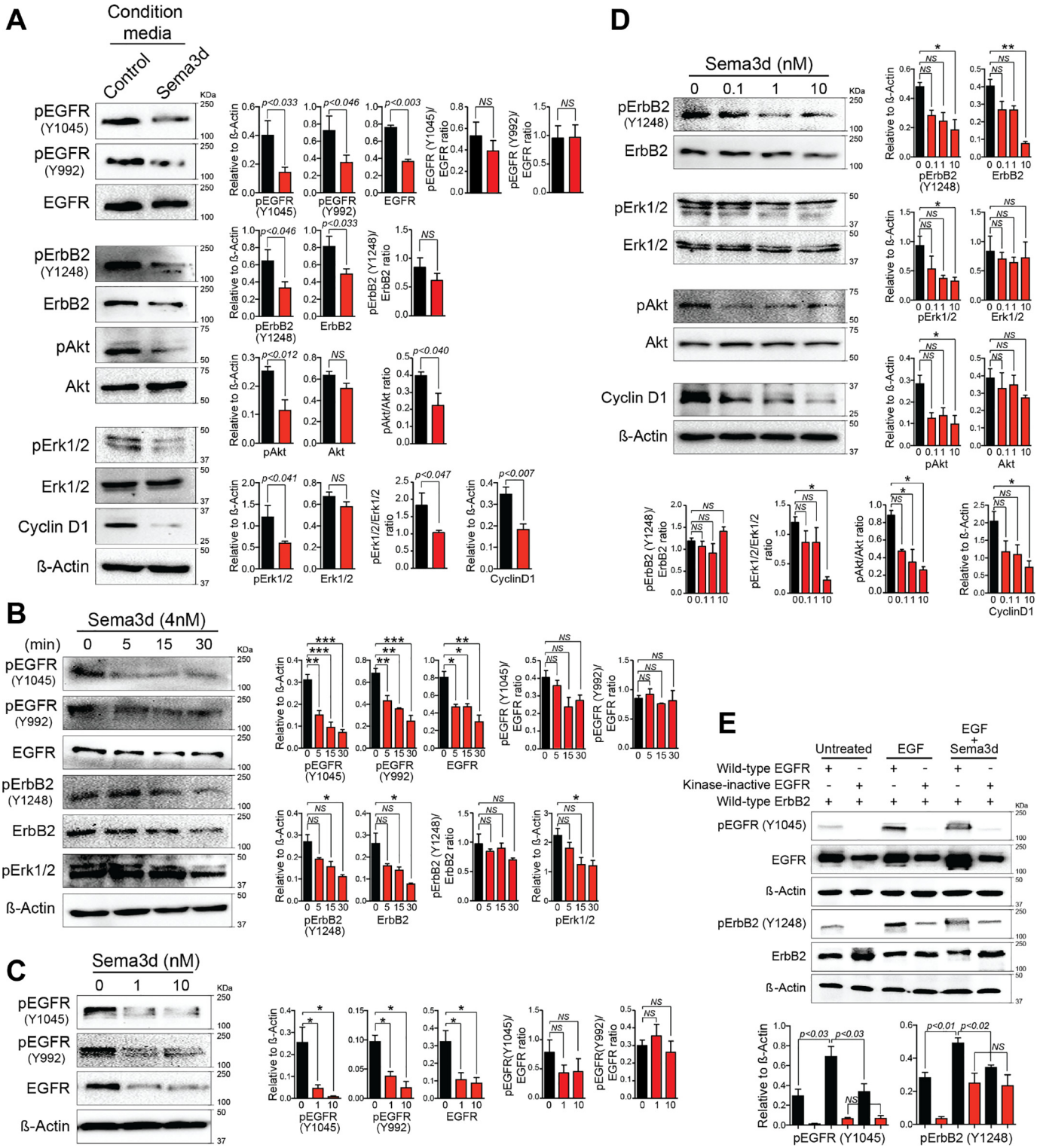

Figure 4. Sema3d inhibits parathyroid cell proliferation by decreasing the EGFR signaling pathway. *A*, Western blotting and quantification for EGFR signaling pathway molecules from sHPT cells incubated with control or Sema3d conditioned medium for 30 min. *B–D*, Western blotting and quantification for EGFR signaling pathway molecules from sHPT cells treated with 4 nM recombinant Sema3d for 0, 5, 15, and 30 min (*B*) or sHPT cells treated with 0, 0.1, 1, and 10 nM recombinant Sema3d for 30 min (*C* and *D*). *, $p < 0.05$; **, $p < 0.01$; ***, $p < 0.001$; *NS*, not significant (one-way ANOVA between groups, post hoc multiple comparisons, Tukey's test). *E*, EGFR signaling in cells expressing mixed WT and kinase-inactive EGFR/ErbB2 heterodimers. HEK293T cells expressing the indicated pairs of EGFR and ErbB2 receptors were treated with recombinant EGF with and without recombinant Sema3d for 30 min. Cell lysates were prepared for Western blots to detect pEGFR, EGFR, pErbB2, ErbB2, and β-actin levels. Western blots were quantified for pEGFR and pErbB2 relative to β-actin levels. *Six bars* in the graph represent six conditions *labeled above* the *blots*. Experiments were repeated three times and quantified. *Error bars*, S.D.

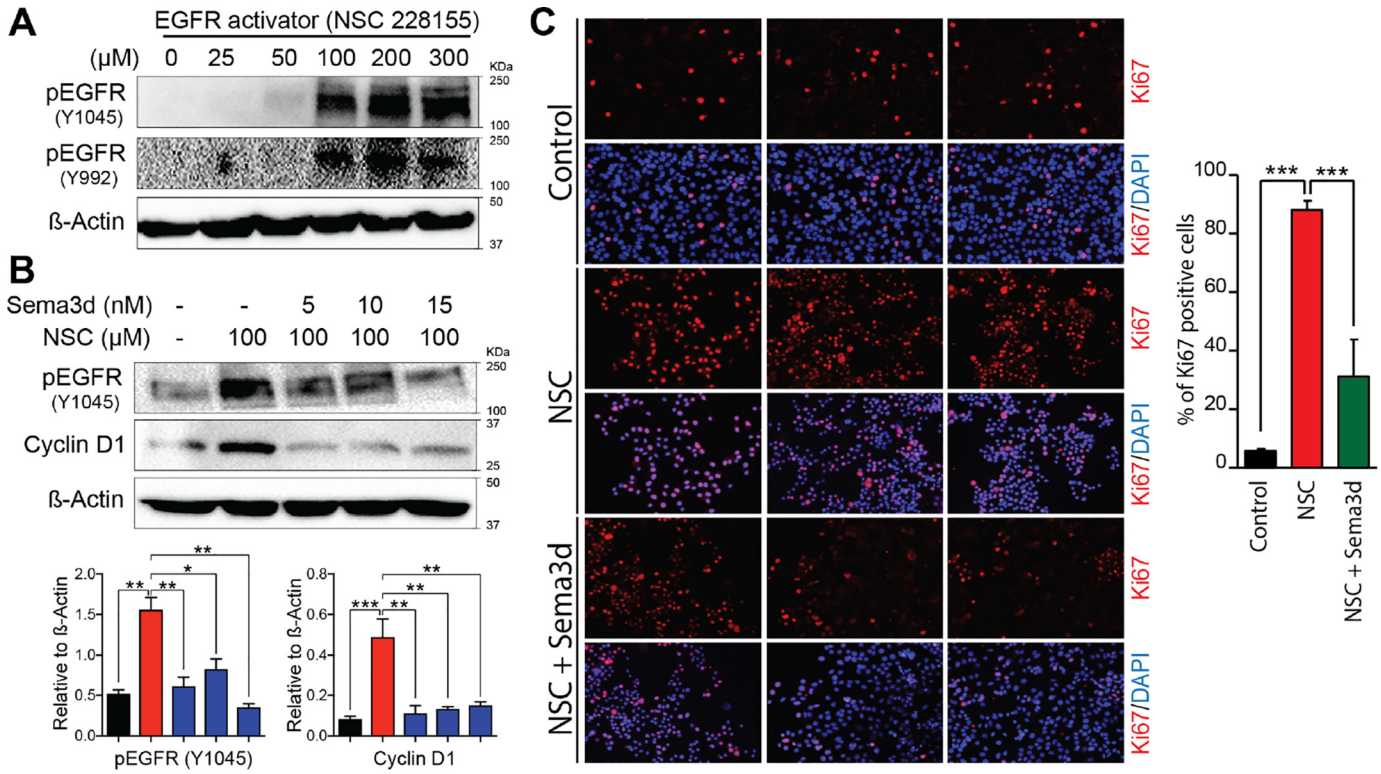

Figure 5. Sema3d inhibits chemically induced EGFR signaling pathway. *A*, optimizing NSC 228155 concentrations to activate the EGFR signaling pathway in sHPT cells. Western blotting for pEGFRs from sHPT cells incubated with increasing concentrations of NSC 228155 for 30 min. *B*, Western blotting and quantification for pEGFR and cyclin D1 from sHPT cells incubated with 100 μM NSC 228155 with or without increasing amounts of recombinant Sema3d (5, 10, and 12 nM) for 30 min. *, $p < 0.05$; **, $p < 0.01$; ***, $p < 0.001$ (one-way ANOVA between groups, post hoc multiple comparisons, Tukey's test). *C*, immunostaining for Ki-67 on sHPT cells treated with either control or NSC 228155 (100 μM) or NSC 228155 (100 μM) together with 10 nM recombinant Sema3d for 24 h. Nuclei were visualized by DAPI staining (*blue*), and the percentage of Ki-67–positive cells was quantified. Experiments were repeated three times and quantified. ***, $p < 0.001$ (one-way ANOVA between groups, post hoc multiple comparisons, Tukey's test). *Error bars*, S.D.

thyroid sections from control and *Sema3d*$^{-/-}$ mice. We observed elevated levels of pEGFR in *Sema3d*$^{-/-}$ parathyroid sections compared with controls (Fig. 6*A*). Next, we tried to determine whether hyperplasia seen in *Sema3d*$^{-/-}$ mice was due to an abnormal increase in the EGFR signaling and whether blocking EGFR signaling can rescue the hyperplasia phenotype. To examine whether elevated EGFR signaling resulted in parathyroid hyperplasia, we treated *Sema3d*$^{-/-}$ mice with either vehicle or erlotinib, an EGFR signaling pathway inhibitor, and analyzed their parathyroid glands. We observed a significant size reduction of the parathyroid glands in *Sema3d*$^{-/-}$ mice treated with erlotinib compared with vehicle-treated controls (Fig. 6*B*). Consistent with reduced parathyroid size, we also observed that Ki-67–positive cells were reduced in erlotinib-treated samples when compared with controls (Fig. 6*C*). To determine whether the reduced parathyroid glands impact PTH levels, we measured serum PTH levels in *Sema3d*$^{-/-}$ mice treated either with vehicle or erlotinib. PTH levels were significantly reduced after erlotinib treatment (Fig. 6*D*). Together, these results indicate that blocking EGFR signaling could partially rescue the hyperplasia and hyperparathyroidism phenotype seen in *Sema3d*$^{-/-}$ mice.

Discussion

The pathogenesis of parathyroid gland hyperplasia in hyperparathyroidism is poorly understood. Thus, a better molecular understanding is essential for prevention and therapeutic intervention. In this study, we demonstrate that *Sema3d*$^{-/-}$ mice develop PHPT from parathyroid hyperplasia. However, only ~40% of *Sema3d*$^{-/-}$ mice develop hyperplasia. We suspect that this incomplete phenotype is contributed by the genetic background, as phenotypes in other class 3 semaphorin knockouts are also strain-dependent (51). Expression of parathyroid-specific developmental genes such as *PTH* and *Gcm2* was increased in *Sema3d*$^{-/-}$ mice. However, CaSR expression was not altered. Expression of CaSR enables the parathyroid cell to respond to changes in extracellular calcium concentration. CaSR activation by high extracellular calcium results in reduced PTH secretion. On the other hand, deactivation of CaSR by low extracellular calcium induces PTH secretion. Normal expression of *CaSR* in *Sema3d*$^{-/-}$ mice suggests that elevated PTH levels are primarily caused by increased gland size and not from individual parathyroid cells secreting more PTH.

Genetic inactivation of *Sema3d* leads to an activated EGFR signaling pathway and cyclin D1, a cell cycle regulator and an oncogene. This results in increased parathyroid cell proliferation. Cyclin D1 binds and activates CDKs that phosphorylate several downstream proteins to ensure cell cycle progression through the G_1/S checkpoint. The role of cyclin D1 in parathyroid tumorigenesis is well-established. Cyclin D1 is overexpressed in 20–40% of parathyroid adenomas (33–35). However, these numbers are much higher (~80%) in sporadic parathyroid adenomas from Asian Indians. Cyclin D1 is also

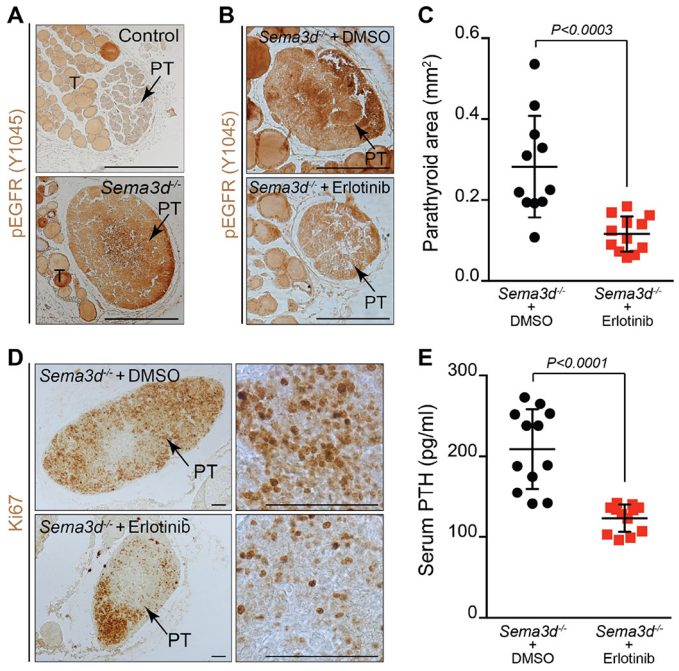

Figure 6. Inhibition of EGFR signaling in *Sema3d* mutants can partially rescue the parathyroid hyperplasia phenotype. *A*, immunohistochemistry for pEGFR on parathyroid sections from 6-month-old control and *Sema3d*$^{-/-}$ mice. *Scale bars*, 200 μm. *B*, immunohistochemistry for pEGFR on parathyroid sections from *Sema3d*$^{-/-}$ mice treated either with either vehicle ($n = 5$) or erlotinib ($n = 5$). *Scale bars*, 200 μm. *C*, decreased parathyroid area in *Sema3d*$^{-/-}$ mice treated with EGFR inhibitor, erlotinib ($n = 12$), compared with vehicle (DMSO)-treated controls ($n = 12$). *D*, immunohistochemistry for Ki-67 on parathyroid sections from *Sema3d*$^{-/-}$ mice treated either with vehicle ($n = 5$) or erlotinib ($n = 5$). High-magnification images show nuclear Ki-67 staining. *Scale bars*, 50 μm. *E*, serum PTH levels in *Sema3d*$^{-/-}$ mice treated either with vehicle ($n = 12$) or erlotinib ($n = 12$). *T*, thyroid; *PT*, parathyroid.

activated in a subset of parathyroid adenomas from chromosomal rearrangement, bringing *the c*yclin D1 gene under the influence of the *PTH* promoter region (34). Studies in transgenic mice have demonstrated that targeted overexpression of cyclin D1 in parathyroid tissues can lead to parathyroid adenomas (33).

Semaphorins signal through their classical plexin and neuropilin receptors. However, semaphorins can also signal through other receptors, such as receptor tyrosine kinases (28, 40, 41). Our data suggest that Sema3d can modulate cell behavior by regulating receptor tyrosine kinases activities. Growth factor receptor tyrosine kinases, including EGFR and ErbB2, play an important role in mediating cancer growth and survival. EGFR is a member of the ErbB family of receptor tyrosine kinases that also includes ErbB2, ErbB3, and ErbB4. Upon ligand binding, ErbB family members can form homo- or heterodimer and activate downstream mitogen-activated protein kinase and the phosphatidylinositol 3-kinase/Akt signaling pathway to regulate cell proliferation. Our data demonstrate that Sema3d can inhibit both EGFR and ErbB2 signaling pathways. Down-regulation of both total and phosphorylated form of EGFR suggests that Sema3d may inhibit EGFR signaling by inducing receptor endocytosis/internalization and degradation. Different post-translational modifications, such as tyrosine and serine/threonine phosphorylation, ubiquitylation, and acetylation, regulate EGF receptor endocytosis (52). Among the class 3 semaphorins, both Sema3a and Sema3e induce endocytosis of plexin receptor/receptor complex during axon guidance (53, 54). Recent work by Aghajanian *et al.* (29) demonstrated that Sema3d does not bind to ErbB2 alone. However, it can bind as part of a receptor complex, suggesting that inhibitory effects of Sema3d on ErbB2 activation are likely from the EGFR signaling pathway (29). Using plasmids expressing either the WT or kinase-inactive form of EGFR, we demonstrate that the inhibitory effects of Sema3d on ErbB2 are EGFR-dependent. In contrast to the inhibitory effect of Sema3d on RTKs, another class 3 semaphorin, Sema3C, can activate RTKs during prostate cancer progression. This suggests that, depending upon its biological context, class 3 semaphorins can act as either agonists or antagonists on the RTK pathway (40).

Our results demonstrate that pharmacological blocking of EGFR signaling can partially rescue the parathyroid hyperplasia phenotype seen in Sema3d knockout mice. It would be interesting to explore whether Sema3d-EGFR signaling can be therapeutically targeted to inhibit parathyroid hyperplasia in both PHPT and SHPT conditions. Parathyroidectomy is the most common treatment for hyperparathyroidism. Because the neck's anatomy was distorted with fibrosis following the initial surgery, there were technical challenges in identifying and safely removing the abnormal parathyroid glands. Therefore, pharmacological treatment for persistent or recurrent hyperparathyroidism may be a good option to address this issue. Administration of EGFR inhibitors has shown beneficial effects. However, systemic inhibition could also suppress renal EGFR signaling and compromise kidney function (49). In contrast to its broad expression during embryonic development, Sema3d expression in adults is enriched in the spleen and thyroid gland (55). In this context, Sema3d may be a potential therapeutic target to treat parathyroid hyperplasia, given its more limited tissue expression in adult mice. Nonetheless, the possible off-target effects of systemic or targeted delivery of Sema3d need to be determined.

Because class 3 semaphorins are secreted proteins, it is possible to use recombinant semaphorins or derived peptides to inhibit parathyroid cell proliferation causing hyperplasia. A recent study by Casazza *et al.* (56) demonstrated that systemic and targeted delivery of Sema3A inhibits tumor progression in multiple mouse models. However, the inhibitory effect of systemic or targeted Sema3d delivery on parathyroid tumor progression remains to be investigated. Our finding that Sema3d inhibits EGFR signaling to restrict aberrant parathyroid tumor cell proliferation may also be relevant to other tumor types. Aberrant activation or overexpression of EGFR is reported in many tumors (57). For example, overexpression of EGFR is observed in 60% of the high-grade gliomas (glioblastoma) (58). SEMA3D has been shown to inhibit glioblastoma growth. The *SEMA3D* expression is reduced in glioblastoma as compared with low-grade gliomas, suggesting that its loss is involved in tumor progression (59). However, the signaling pathways mediating these effects of SEMA3D in gliomas have not been identified. Thus, future work in this direction is required for the development of anti-tumor therapeutic strategies targeting the semaphorin signaling pathway.

Experimental procedures

Experimental animals

All mice were maintained on a mixed (C57BL/6 and Sv/129) genetic background. Both male and female mice were used for analysis. *Sema3d*^{GFPCre} allele has been described previously (30, 60). Heterozygous mice (*Sema3d*$^{GFPCre/+}$) were crossed together to generate *Sema3d*$^{GFPCre/GFPCre}$ (*Sema3d*$^{-/-}$) mice. *Sema3d*$^{+/+}$ or *Sema3d*$^{GFPCre/+}$ mice were used as control. The SingHealth institutional animal care and use committee approved all animal protocols.

Histology and immunohistochemistry

After genotyping of the pups from *Sema3d* heterozygous intercross, we randomly selected 12 control and 12 *Sema3d*$^{-/-}$ mice from the cohort for histological analysis. Histology and immunohistochemistry were performed as described previously (61–65). Briefly, the thyroid, parathyroids, and trachea tissues were dissected en bloc in PBS and fixed in 4% paraformaldehyde overnight at 4 °C. The tissues were washed with PBS, dehydrated in an ethanol series, and stored in 100% ethanol at 20 °C. To examine the parathyroid glands, serial paraffin sections were cut to a thickness of 5–10 μm and processed for either morphological hematoxylin/eosin staining or immunohistochemistry. For immunohistochemistry, the sections were deparaffinized in xylenes, and slides were deparaffinized in xylene, dehydrated in ethanol, and rehydrated in water. Antigen retrieval using Bull's eye decloaker (Biocare Medicals, catalogue no. BULL1000 MX) or Tris-based solution (Vector Laboratories, catalog no. H-3301) was performed according to the manufacturer's instructions. Endogenous peroxidase activity was blocked with hydrogen peroxide (3%) treatment. Slides were washed in PBS and blocked in blocking buffer (5% serum) for 1–2 h at room temperature. Slides were incubated overnight with primary antibody diluted in blocking buffer. The next day, slides were washed, and a secondary antibody was applied for 2 h at room temperature. Primary antibodies used were anti-GCM2 goat polyclonal (Santa Cruz Biotechnology, Inc., catalogue no. sc-79495), anti-Ki-67 rabbit monoclonal (Abcam, catalogue no. ab16667), and anti-pEGFR-Y1045 rabbit polyclonal (Cell signaling, catalogue no. 2237). Secondary antibodies used were ImmPRESS® horseradish peroxidase anti-goat (Vector Laboratories, catalogue no. MP-7405-50) or anti-rabbit (Vector Laboratories, catalogue no. MP-7401-50). The sections were washed, and staining was visualized using the DAB substrate kit (Vector Laboratories, catalogue no. SK-4100).

Biochemical analyses

At the indicated age, control and *Sema3d*$^{-/-}$ mice were anesthetized, and blood was collected by cardiac puncture for plasma separation. Plasma PTH levels were measured using the mouse intact PTH ELISA kits (Immutopics, Inc., catalogue no. 60-2300). Plasma calcium levels were measured using a calcium detection kit (Abcam, catalogue no. ab102505).

sHPT cell culture

Human parathyroid tumor cell line sHPT-1 was established by Björklund *et al.* (39), as previously described. sHPT-1 cells were cultured and expanded in Dulbecco's modified Eagle's medium (DMEM) (Gibco, catalogue no. 11965-092) containing 1% penicillin/streptomycin and 10% FBS. After reaching 70–80% confluence, cells were cultured and starved overnight in DMEM supplemented with 1% penicillin/streptomycin and 1% FBS. They were subsequently treated with Sema3d conditioned medium or recombinant Sema3d (Abnova, catalogue no. H00223117-P01) in the desired concentrations at the indicated time points with appropriate controls. For the proliferation assay, sHPT-1 cells were treated with or without recombinant Sema3d at 10 nM for 48 h. In another experiment, sHPT-1 cells were stimulated with NSC 228155 (100 μM) or in combination with 10 nM recombinant Sema3d for 24 h. After treatment, cells were fixed with 4% paraformaldehyde for 30 min at room temperature and evaluated for cell proliferation by Ki-67 (eBioscience, catalogue no. 14-5698-82) immunofluorescence staining. Briefly, cells were fixed and washed with PBS and incubated for 2 h at room temperature with Ki-67 antibody diluted at a concentration of 5 μg/ml in PBS containing 2% BSA. After washing with PBS, cells were incubated for 30 min at room temperature with goat anti-rat IgG, Alexa Fluor 586 (Invitrogen, catalogue no. A-11077). The cells were then washed again and incubated with DAPI for nuclear staining visualized with fluorescence microscopy (Olympus IX71S1F3).

EGFR activation assay

sHPT-1 cells were incubated with either DMSO as vehicle or NSC 228155 compound (Calbiochem, catalogue no. 5.30536.0001CN) for 30 min at 25, 50, 100, 200, and 300 μM and analyzed for EGFR members by Western blotting. In another experiment, sHPT-1 cells were treated with either NSC 228155 (100 μM) or in combination with recombinant Sema3d (5, 10, and 15 nM) for 30 min and analyzed for EGFR with Western blot analysis.

Mice and erlotinib

12-week-old *Sema3d*$^{-/-}$ mice were randomly assigned to two treatment groups: vehicle (DMSO) and erlotinib (10 mg/kg body weight) (Selleckchem, catalogue no. S1023). Treatments were administered every 2 days by intraperitoneal injection. After 4 weeks of treatment, the mice were sacrificed, and serum and parathyroid tissue were collected for histologic and molecular analyses.

Preparation of Sema3d conditioned medium

HEK293T cells were cultured and expanded in DMEM (Gibco, catalogue no. 11965-092) supplemented with 1% penicillin/streptomycin and 10% FBS. HEK293T cells were transfected with either Sema3d pAP-Tag4 or empty vector plasmid using the FuGENE® 6 transfection reagent (Promega, catalogue no. E2691) according to the manufacturer's protocol. After 24 h, the conditioned medium was changed to DMEM (Gibco, catalogue no. 11965-092) supplemented with 1% penicillin/streptomycin and 0.5% FBS. The cells were then incubated for 72 h, and the conditioned medium was collected. The conditioned medium was filtered using a 0.2-μm syringe filter and centrifuged at 5000 rpm for 5 min. AP activity in the conditioned medium was measured with a colorimetric assay as

described previously (30). The conditioned medium was then used for the experiments.

Kinase activation assay

HEK293T cells were transfected with either plasmid expressing WT ErbB2, a WT EGFR, or a kinase-inactive EGFR (K721A) using Lipofectamine transfection reagent (Thermo Fisher Scientific, catalogue no. 11668019) according to the manufacturer's protocol. Following transient transfection, cells were incubated for 48 h and starved for 4 h with serum-free DMEM supplemented with 1% penicillin/streptomycin. Cells were then treated with/without 200 ng/ml EGF (PeproTech, catalogue no. AF-100-15) and with/without 10 nM recombinant Sema3d for 30 min. Cell lysates were collected for Western blot analysis. Plasmids expressing WT EGFR and kinase-inactive EGFR (K721A) were kindly provided by Sara Sigismund from Pier Paolo Di Fiore's laboratory (European Institute of Oncology, Milan, Italy). The plasmid expressing ErbB2 was a gift from Martin Offterdinger (Addgene plasmid 40268) (66).

RNA extraction and quantitative RT-PCR

Parathyroid glands were dissected from control and *Sema3d*$^{-/-}$ mice. Because only ~40% of the *Sema3d*$^{-/-}$ mice had parathyroid hyperplasia, we decided to use hyperplastic (enlarged) parathyroid tissue from *Sema3d*$^{-/-}$ mice. Total RNA was isolated from glands using TRIzol (Life Technologies, Inc., catalogue no. 15596-018). RNA was reverse-transcribed using random hexamers and the SuperScript III First-Strand Synthesis system (Life Technologies, catalogue no. 18080-051). Gene expression was measured by quantitative RT-PCR (ABI PRISM 7900 or ViiA7 Real-Time PCR System) using the Power SYBR Green master mix (Life Technologies, catalogue no. 4368702). Both signals and relative gene expression were normalized to corresponding glyceraldehyde-3-phosphate dehydrogenase controls. PCR conditions and primer set sequences are available upon request.

Western blotting analyses

Western blots were performed as described previously (61, 67). Briefly, cells were washed twice with cold Dulbecco's PBS (Lonza, catalogue no. 17-512F) and lysed with radioimmune precipitation assay buffer (Thermo Scientific, catalogue no. 89901) containing 1:100 diluted protease and phosphatase inhibitor mixture (Sigma). The cell lysates were centrifuged at 13,000 rpm for 10 min at 4 °C, and the supernatant was collected for immunoblot analyses. Total protein concentration was determined with a Pierce BCA protein assay kit (Thermo Scientific, catalogue no. 23225) following the manufacturer's instructions. Approximately 20–30 μg of total protein samples were separated by SDS-PAGE and transferred to nitrocellulose membrane using the Trans-Blot Turbo system (Bio-Rad). Membranes were then blocked with 2–5% BSA in TBS containing 0.1% Tween (TBST) and subsequently incubated with primary antibodies diluted in TBST containing 2–5% BSA overnight at 4 °C. Blots were then washed in TBST and incubated for 1.5 h at room temperature probed with the appropriate horseradish peroxidase–linked secondary antibodies (Santa Cruz Biotechnology). Immunoreactive bands were detected by chemiluminescence (Hiss GmbH, catalogue no. 16026) using the Gel Doc XR+ System (Bio-Rad). All experiments were repeated three times and quantified. Primary antibodies used for immunoblot analyses were pAkt (Cell Signaling, catalogue no. 4060S), Akt (Cell Signaling, catalogue no. 9272S), pErk1/2 (Cell Signaling, catalogue no. 9101S), Erk1/2 (Cell Signaling, catalogue no. 9102S), pErbB2 (Cell Signaling, catalogue no. 2247), ErbB2 (Cell Signaling, catalogue no. 2242), cyclin D1 (Santa Cruz Biotechnology, catalogue no. sc-8396), pEGFR-Y1045 (Cell Signaling, catalogue no. 2237), pEGFR-Y992 (Cell Signaling, catalogue no. 2235), EGFR (Cell Signaling, catalogue no. 4267), vinculin (Sigma, catalogue no. V9131), glyceraldehyde-3-phosphate dehydrogenase (Santa Cruz Biotechnology, catalogue no. sc-20357), and β-actin (Santa Cruz Biotechnology, catalogue no. sc-47778).

Statistical analyses

Statistical analyses were performed using two-tailed Student's *t* test. Data were expressed as mean ± S.D. Differences were considered significant with $p < 0.05$. One-way analysis of variance (ANOVA) was used to assess statistical differences between groups. Significant ANOVA results were further analyzed by Tukey's multiple-comparison test (*, $p < 0.05$; **, $p < 0.01$; ***, $p < 0.001$; *NS*, not significant).

Author contributions—A. S., M. M. M., D. M. C., A. K. A., S. K. B., and M. K. S. designed and performed experiments and analyzed the data. M. K. S. oversaw the entire project, designed experiments, analyzed data, and wrote the paper. All authors reviewed the results and approved the final version of the manuscript.

Acknowledgments—We are thankful to Jonathan A. Epstein (University of Pennsylvania, Philadelphia, PA) for providing Sema3d$^{GFPCre/+}$ *mice and Gunnar Westin (Uppsala University) for the sHPT-1 cell line. We thank Shamini Guna Shekeran for technical support.*

References

1. Rodan, G. A., and Martin, T. J. (2000) Therapeutic approaches to bone diseases. *Science* **289,** 1508–1514 CrossRef Medline
2. Stewart, A. F., Cain, R. L., Burr, D. B., Jacob, D., Turner, C. H., and Hock, J. M. (2000) Six-month daily administration of parathyroid hormone and parathyroid hormone-related protein peptides to adult ovariectomized rats markedly enhances bone mass and biomechanical properties: a comparison of human parathyroid hormone 1–34, parathyroid hormone-related protein 1–36, and SDZ-parathyroid hormone 893. *J. Bone Miner. Res.* **15,** 1517–1525 CrossRef Medline
3. Dempster, D. W., Cosman, F., Kurland, E. S., Zhou, H., Nieves, J., Woelfert, L., Shane, E., Plavetić, K., Müller, R., Bilezikian, J., and Lindsay, R. (2001) Effects of daily treatment with parathyroid hormone on bone microarchitecture and turnover in patients with osteoporosis: a paired biopsy study. *J. Bone Miner. Res.* **16,** 1846–1853 CrossRef Medline
4. Neer, R. M., Arnaud, C. D., Zanchetta, J. R., Prince, R., Gaich, G. A., Reginster, J. Y., Hodsman, A. B., Eriksen, E. F., Ish-Shalom, S., Genant, H. K., Wang, O., and Mitlak, B. H. (2001) Effect of parathyroid hormone (1–34) on fractures and bone mineral density in postmenopausal women with osteoporosis. *N. Engl. J. Med.* **344,** 1434–1441 CrossRef Medline
5. Moore-Scott, B. A., and Manley, N. R. (2005) Differential expression of Sonic hedgehog along the anterior-posterior axis regulates patterning of pharyngeal pouch endoderm and pharyngeal endoderm-derived organs. *Dev. Biol.* **278,** 323–335 CrossRef Medline

6. Cordier, A. C., and Haumont, S. M. (1980) Development of thymus, parathyroids, and ultimo-branchial bodies in NMRI and nude mice. *Am. J. Anat.* **157,** 227–263 CrossRef Medline
7. Manley, N. R., and Capecchi, M. R. (1998) Hox group 3 paralogs regulate the development and migration of the thymus, thyroid, and parathyroid glands. *Dev. Biol.* **195,** 1–15 CrossRef Medline
8. Gordon, J., Bennett, A. R., Blackburn, C. C., and Manley, N. R. (2001) Gcm2 and Foxn1 mark early parathyroid- and thymus-specific domains in the developing third pharyngeal pouch. *Mech. Dev.* **103,** 141–143 CrossRef Medline
9. Grigorieva, I. V., Mirczuk, S., Gaynor, K. U., Nesbit, M. A., Grigorieva, E. F., Wei, Q., Ali, A., Fairclough, R. J., Stacey, J. M., Stechman, M. J., Mihai, R., Kurek, D., Fraser, W. D., Hough, T., Condie, B. G., *et al.* (2010) Gata3-deficient mice develop parathyroid abnormalities due to dysregulation of the parathyroid-specific transcription factor Gcm2. *J. Clin. Invest.* **120,** 2144–2155 CrossRef Medline
10. Manley, N. R., and Capecchi, M. R. (1995) The role of Hoxa-3 in mouse thymus and thyroid development. *Development* **121,** 1989–2003 Medline
11. Wallin, J., Eibel, H., Neubüser, A., Wilting, J., Koseki, H., and Balling, R. (1996) Pax1 is expressed during development of the thymus epithelium and is required for normal T-cell maturation. *Development* **122,** 23–30 Medline
12. Blackburn, C. C., and Manley, N. R. (2004) Developing a new paradigm for thymus organogenesis. *Nat. Rev. Immunol.* **4,** 278–289 CrossRef Medline
13. Dietrich, S., and Gruss, P. (1995) Undulated phenotypes suggest a role of Pax-1 for the development of vertebral and extravertebral structures. *Dev. Biol.* **167,** 529–548 CrossRef Medline
14. Günther, T., Chen, Z. F., Kim, J., Priemel, M., Rueger, J. M., Amling, M., Moseley, J. M., Martin, T. J., Anderson, D. J., and Karsenty, G. (2000) Genetic ablation of parathyroid glands reveals another source of parathyroid hormone. *Nature* **406,** 199–203 CrossRef Medline
15. Liu, Z., Yu, S., and Manley, N. R. (2007) Gcm2 is required for the differentiation and survival of parathyroid precursor cells in the parathyroid/thymus primordia. *Dev. Biol.* **305,** 333–346 CrossRef Medline
16. Walker, M. D., and Silverberg, S. J. (2018) Primary hyperparathyroidism. *Nat. Rev. Endocrinol.* **14,** 115–125 CrossRef Medline
17. Bilezikian, J. P., Bandeira, L., Khan, A., and Cusano, N. E. (2018) Hyperparathyroidism. *Lancet* **391,** 168–178 CrossRef Medline
18. Bandeira, L., and Bilezikian, J. (2016) Primary hyperparathyroidism. *F1000Res.* **5,** F1000 Faculty Rev-1 CrossRef Medline
19. Marcocci, C., Cetani, F., Rubin, M. R., Silverberg, S. J., Pinchera, A., and Bilezikian, J. P. (2008) Parathyroid carcinoma. *J. Bone Miner. Res.* **23,** 1869–1880 CrossRef Medline
20. Bilezikian, J. P., Cusano, N. E., Khan, A. A., Liu, J. M., Marcocci, C., and Bandeira, F. (2016) Primary hyperparathyroidism. *Nat. Rev. Dis. Primers* **2,** 16033 CrossRef Medline
21. Torres, P. U., Prié, D., Beck, L., and Friedlander, G. (2006) New therapies for uremic secondary hyperparathyroidism. *J. Ren. Nutr.* **16,** 87–99 CrossRef Medline
22. Prescott, J. D., and Udelsman, R. (2009) Remedial operation for primary hyperparathyroidism. *World J. Surg.* **33,** 2324–2334 CrossRef Medline
23. Pasterkamp, R. J. (2012) Getting neural circuits into shape with semaphorins. *Nat. Rev. Neurosci.* **13,** 605–618 CrossRef Medline
24. Neufeld, G., Mumblat, Y., Smolkin, T., Toledano, S., Nir-Zvi, I., Ziv, K., and Kessler, O. (2016) The semaphorins and their receptors as modulators of tumor progression. *Drug Resist. Updat.* **29,** 1–12 CrossRef Medline
25. Tamagnone, L. (2012) Emerging role of semaphorins as major regulatory signals and potential therapeutic targets in cancer. *Cancer Cell* **22,** 145–152 CrossRef Medline
26. Epstein, J. A., Aghajanian, H., and Singh, M. K. (2015) Semaphorin signaling in cardiovascular development. *Cell Metab.* **21,** 163–173 CrossRef Medline
27. Worzfeld, T., and Offermanns, S. (2014) Semaphorins and plexins as therapeutic targets. *Nat. Rev. Drug Discov.* **13,** 603–621 CrossRef Medline
28. Cagnoni, G., and Tamagnone, L. (2014) Semaphorin receptors meet receptor tyrosine kinases on the way of tumor progression. *Oncogene* **33,** 4795–4802 CrossRef Medline
29. Aghajanian, H., Cho, Y. K., Manderfield, L. J., Herling, M. R., Gupta, M., Ho, V. C., Li, L., Degenhardt, K., Aharonov, A., Tzahor, E., and Epstein, J. A. (2016) Coronary vasculature patterning requires a novel endothelial ErbB2 holoreceptor. *Nat. Commun.* **7,** 12038 CrossRef Medline
30. Degenhardt, K., Singh, M. K., Aghajanian, H., Massera, D., Wang, Q., Li, J., Li, L., Choi, C., Yzaguirre, A. D., Francey, L. J., Gallant, E., Krantz, I. D., Gruber, P. J., and Epstein, J. A. (2013) Semaphorin 3d signaling defects are associated with anomalous pulmonary venous connections. *Nat. Med.* **19,** 760–765 CrossRef Medline
31. Takahashi, K., Ishida, M., Hirokawa, K., and Takahashi, H. (2008) Expression of the semaphorins Sema 3D and Sema 3F in the developing parathyroid and thymus. *Dev. Dyn.* **237,** 1699–1708 CrossRef Medline
32. Cusano, N. E., Silverberg, S. J., and Bilezikian, J. P. (2013) Normocalcemic primary hyperparathyroidism. *J. Clin. Densitom.* **16,** 33–39 CrossRef Medline
33. Imanishi, Y., Hosokawa, Y., Yoshimoto, K., Schipani, E., Mallya, S., Papanikolaou, A., Kifor, O., Tokura, T., Sablosky, M., Ledgard, F., Gronowicz, G., Wang, T. C., Schmidt, E. V., Hall, C., Brown, E. M., *et al.* (2001) Primary hyperparathyroidism caused by parathyroid-targeted overexpression of cyclin D1 in transgenic mice. *J. Clin. Invest.* **107,** 1093–1102 CrossRef Medline
34. Hsi, E. D., Zukerberg, L. R., Yang, W. I., and Arnold, A. (1996) Cyclin D1/PRAD1 expression in parathyroid adenomas: an immunohistochemical study. *J. Clin. Endocrinol. Metab.* **81,** 1736–1739 CrossRef Medline
35. Tominaga, Y., Tsuzuki, T., Uchida, K., Haba, T., Otsuka, S., Ichimori, T., Yamada, K., Numano, M., Tanaka, Y., and Takagi, H. (1999) Expression of PRAD1/cyclin D1, retinoblastoma gene products, and Ki67 in parathyroid hyperplasia caused by chronic renal failure versus primary adenoma. *Kidney Int.* **55,** 1375–1383 CrossRef Medline
36. Dong, Y., Walsh, M. D., McGuckin, M. A., Gabrielli, B. G., Cummings, M. C., Wright, R. G., Hurst, T., Khoo, S. K., and Parsons, P. G. (1997) Increased expression of cyclin-dependent kinase inhibitor 2 (CDKN2A) gene product P16INK4A in ovarian cancer is associated with progression and unfavourable prognosis. *Int. J. Cancer* **74,** 57–63 CrossRef Medline
37. Abbas, T., and Dutta, A. (2009) p21 in cancer: intricate networks and multiple activities. *Nat. Rev. Cancer* **9,** 400–414 CrossRef Medline
38. Roninson, I. B. (2002) Oncogenic functions of tumour suppressor p21(Waf1/Cip1/Sdi1): association with cell senescence and tumour-promoting activities of stromal fibroblasts. *Cancer Lett.* **179,** 1–14 CrossRef Medline
39. Björklund, P., Akerström, G., and Westin, G. (2007) Activated β-catenin in the novel human parathyroid tumor cell line sHPT-1. *Biochem. Biophys. Res. Commun.* **352,** 532–536 CrossRef Medline
40. Peacock, J. W., Takeuchi, A., Hayashi, N., Liu, L., Tam, K. J., Al Nakouzi, N., Khazamipour, N., Tombe, T., Dejima, T., Lee, K. C., Shiota, M., Thaper, D., Lee, W. C., Hui, D. H., Kuruma, H., *et al.* (2018) SEMA3C drives cancer growth by transactivating multiple receptor tyrosine kinases via Plexin B1. *EMBO Mol. Med.* **10,** 219–238 CrossRef Medline
41. Worzfeld, T., Swiercz, J. M., Looso, M., Straub, B. K., Sivaraj, K. K., and Offermanns, S. (2012) ErbB-2 signals through Plexin-B1 to promote breast cancer metastasis. *J. Clin. Invest.* **122,** 1296–1305 CrossRef Medline
42. Aghajanian, H., Choi, C., Ho, V. C., Gupta, M., Singh, M. K., and Epstein, J. A. (2014) Semaphorin 3d and Semaphorin 3e direct endothelial motility through distinct molecular signaling pathways. *J. Biol. Chem.* **289,** 17971–17979 CrossRef Medline
43. Lenferink, A. E., Busse, D., Flanagan, W. M., Yakes, F. M., and Arteaga, C. L. (2001) ErbB2/neu kinase modulates cellular p27(Kip1) and cyclin D1 through multiple signaling pathways. *Cancer Res.* **61,** 6583–6591 Medline
44. Roskoski, R., Jr. (2014) The ErbB/HER family of protein-tyrosine kinases and cancer. *Pharmacol. Res.* **79,** 34–74 CrossRef Medline
45. Bednarz, N., Błaut, K., Sworczak, K., Oseka, T., and Bielawski, K. P. (2009) The profile of ErbB/Her family genes copy number assessed by real-time PCR in parathyroid adenoma and hyperplasia associated with sporadic primary hyperparathyroidism. *Acta Biochim. Pol.* **56,** 83–88 Medline
46. Sadler, G. P., Morgan, J. M., Jasani, B., Douglas-Jones, A., and Wheeler, M. H. (1996) Epidermal growth factor receptor status in hyperparathy-

roidism: immunocytochemical and *in situ* hybridization study. *World J. Surg.* **20,** 736–742; discussion 742–733 CrossRef Medline
47. Gülkesen, K. H., Kiliçarslan, B., Altunbaş, H. A., and Karpuzoglu, G. (2001) EGFR and p53 expression and proliferative activity in parathyroid adenomas: an immunohistochemical study. *APMIS* **109,** 870–874 CrossRef Medline
48. Cozzolino, M., Lu, Y., Sato, T., Yang, J., Suarez, I. G., Brancaccio, D., Slatopolsky, E., and Dusso, A. S. (2005) A critical role for enhanced TGF-α and EGFR expression in the initiation of parathyroid hyperplasia in experimental kidney disease. *Am. J. Physiol. Renal Physiol.* **289,** F1096–F1102 CrossRef Medline
49. Arcidiacono, M. V., Sato, T., Alvarez-Hernandez, D., Yang, J., Tokumoto, M., Gonzalez-Suarez, I., Lu, Y., Tominaga, Y., Cannata-Andia, J., Slatopolsky, E., and Dusso, A. S. (2008) EGFR activation increases parathyroid hyperplasia and calcitriol resistance in kidney disease. *J. Am. Soc. Nephrol.* **19,** 310–320 CrossRef Medline
50. Sakanyan, V., Angelini, M., Le Béchec, M., Lecocq, M. F., Benaiteau, F., Rousseau, B., Gyulkhandanyan, A., Gyulkhandanyan, L., Logé, C., Reiter, E., Roussakis, C., and Fleury, F. (2014) Screening and discovery of nitrobenzoxadiazole compounds activating epidermal growth factor receptor (EGFR) in cancer cells. *Sci. Rep.* **4,** 3977 Medline
51. Feiner, L., Webber, A. L., Brown, C. B., Lu, M. M., Jia, L., Feinstein, P., Mombaerts, P., Epstein, J. A., and Raper, J. A. (2001) Targeted disruption of semaphorin 3C leads to persistent truncus arteriosus and aortic arch interruption. *Development* **128,** 3061–3070 Medline
52. Tong, J., Taylor, P., and Moran, M. F. (2014) Proteomic analysis of the epidermal growth factor receptor (EGFR) interactome and post-translational modifications associated with receptor endocytosis in response to EGF and stress. *Mol. Cell. Proteomics* **13,** 1644–1658 CrossRef Medline
53. Fournier, A. E., Nakamura, F., Kawamoto, S., Goshima, Y., Kalb, R. G., and Strittmatter, S. M. (2000) Semaphorin3A enhances endocytosis at sites of receptor-F-actin colocalization during growth cone collapse. *J. Cell Biol.* **149,** 411–422 CrossRef Medline
54. Burk, K., Mire, E., Bellon, A., Hocine, M., Guillot, J., Moraes, F., Yoshida, Y., Simons, M., Chauvet, S., and Mann, F. (2017) Post-endocytic sorting of Plexin-D1 controls signal transduction and development of axonal and vascular circuits. *Nat. Commun.* **8,** 14508 CrossRef Medline
55. Fagerberg, L., Hallström, B. M., Oksvold, P., Kampf, C., Djureinovic, D., Odeberg, J., Habuka, M., Tahmasebpoor, S., Danielsson, A., Edlund, K., Asplund, A., Sjöstedt, E., Lundberg, E., Szigyarto, C. A., Skogs, M., *et al.* (2014) Analysis of the human tissue-specific expression by genome-wide integration of transcriptomics and antibody-based proteomics. *Mol. Cell. Proteomics* **13,** 397–406 CrossRef Medline
56. Casazza, A., Fu, X., Johansson, I., Capparuccia, L., Andersson, F., Giustacchini, A., Squadrito, M. L., Venneri, M. A., Mazzone, M., Larsson, E., Carmeliet, P., De Palma, M., Naldini, L., Tamagnone, L., and Rolny, C. (2011) Systemic and targeted delivery of semaphorin 3A inhibits tumor angiogenesis and progression in mouse tumor models. *Arterioscler. Thromb. Vasc. Biol.* **31,** 741–749 CrossRef Medline
57. Arteaga, C. L., and Engelman, J. A. (2014) ERBB receptors: from oncogene discovery to basic science to mechanism-based cancer therapeutics. *Cancer Cell* **25,** 282–303 CrossRef Medline
58. Furnari, F. B., Cloughesy, T. F., Cavenee, W. K., and Mischel, P. S. (2015) Heterogeneity of epidermal growth factor receptor signalling networks in glioblastoma. *Nat. Rev. Cancer* **15,** 302–310 CrossRef Medline
59. Karayan-Tapon, L., Wager, M., Guilhot, J., Levillain, P., Marquant, C., Clarhaut, J., Potiron, V., and Roche, J. (2008) Semaphorin, neuropilin and VEGF expression in glial tumours: SEMA3G, a prognostic marker? *Br. J. Cancer* **99,** 1153–1160 CrossRef Medline
60. Katz, T. C., Singh, M. K., Degenhardt, K., Rivera-Feliciano, J., Johnson, R. L., Epstein, J. A., and Tabin, C. J. (2012) Distinct compartments of the proepicardial organ give rise to coronary vascular endothelial cells. *Dev. Cell* **22,** 639–650 CrossRef Medline
61. Singh, A., Ramesh, S., Cibi, D. M., Yun, L. S., Li, J., Li, L., Manderfield, L. J., Olson, E. N., Epstein, J. A., and Singh, M. K. (2016) Hippo signaling mediators Yap and Taz are required in the epicardium for coronary vasculature development. *Cell Rep.* **15,** 1384–1393 CrossRef Medline
62. Singh, M. K., Lu, M. M., Massera, D., and Epstein, J. A. (2011) MicroRNA-processing enzyme Dicer is required in epicardium for coronary vasculature development. *J. Biol. Chem.* **286,** 41036–41045 CrossRef Medline
63. Greicius, G., Kabiri, Z., Sigmundsson, K., Liang, C., Bunte, R., Singh, M. K., and Virshup, D. M. (2018) PDGFRα(+) pericryptal stromal cells are the critical source of Wnts and RSPO3 for murine intestinal stem cells *in vivo*. *Proc. Natl. Acad. Sci. U.S.A.* **115,** E3173–E3181 CrossRef Medline
64. Singh, N., Gupta, M., Trivedi, C. M., Singh, M. K., Li, L., and Epstein, J. A. (2013) Murine craniofacial development requires Hdac3-mediated repression of Msx gene expression. *Dev. Biol.* **377,** 333–344 CrossRef Medline
65. Meadows, S. M., Ratliff, L. A., Singh, M. K., Epstein, J. A., and Cleaver, O. (2013) Resolution of defective dorsal aortae patterning in Sema3E-deficient mice occurs via angiogenic remodeling. *Dev. Dyn.* **242,** 580–590 CrossRef Medline
66. Offterdinger, M., and Bastiaens, P. I. (2008) Prolonged EGFR signaling by ERBB2-mediated sequestration at the plasma membrane. *Traffic* **9,** 147–155 CrossRef Medline
67. Lee, K. Y., Singh, M. K., Ussar, S., Wetzel, P., Hirshman, M. F., Goodyear, L. J., Kispert, A., and Kahn, C. R. (2015) Tbx15 controls skeletal muscle fibre-type determination and muscle metabolism. *Nat. Commun.* **6,** 8054 CrossRef Medline